Epoxy Nanocomposites with Highly Exfoliated Clay: Mechanical Properties and Fracture Mechanisms

Ke Wang,[†,‡] Ling Chen,[†,§] Jingshen Wu,[⊥] Mei Ling Toh,[†,||] Chaobin He,*[,†,#] and Albert F. Yee*[,○]

Institute of Materials Research and Engineering, 3 Research Link, Singapore 117602, Department of Mechanical Engineering, Hong Kong University of Science & Technology, Clearwater Bay Road, Kowloon, Hong Kong, and Department of Materials Science and Engineering, University of Michigan, Ann Arbor, Michigan 48109

ABSTRACT: Epoxy/clay nanocomposites with a better exfoliated morphology have been successfully prepared using a so-called "slurry-compounding" process. The microstructures of the nanocomposites (epoxy/S-clays) were characterized by means of optical microscopy and transmission electron microscopy (TEM). It was found that clay was highly exfoliated and uniformly dispersed in the resulting nanocomposite. Characterizations of mechanical and fracture behaviors revealed that Young's modulus increases monotonically with increasing the clay concentration while the fracture toughness shows a maximum at 2.5 wt % of clay. No *R*-curve behavior was observed in these nanocomposites. The microdeformation and fracture mechanisms were investigated by studying the microstructure of arrested crack tips and the damage zone using TEM and scanning electron microscopy (SEM). The initiation and development of microcracks are the dominant microdeformation and fracture mechanisms in the epoxy/ S-clay nanocomposites. Most of the microcracks initiate between clay layers. The formation of a large number of microcracks and the increase in the fracture surface area due to crack deflection are the major toughening mechanisms.

Introduction

Polymer/layered silicate nanocomposites have been studied extensively as a new generation of polymeric materials.[1−9] Due to the unique nanometer-size dispersion of the layered silicates with high aspect ratios, high surface areas, and high strengths in the polymer matrix, nanocomposites generally exhibit significantly improved properties at very low volume fraction loadings of layered silicates.[1] These properties include mechanical performance, thermal stability, barrier performance, and flame retardancy.

Epoxies are among the best polymeric materials being used in many fields, especially in the aviation industry as adhesives and in structural applications as the matrix materials of fiber-reinforced composites. Since the pioneering work of Pinnavaia's and Giannelis's groups,[2−6] extensive research has been carried out on the preparation and the exfoliation mechanisms of epoxy/layered silicate nanocomposites.[7−16] It has been demonstrated by several groups[10−16] that both Young's modulus and the fracture toughness have been improved with the incorporation of layered silicates. However, there is very little knowledge regarding the deformation and fracture mechanisms. Zilg et al.[10] compared the balance of toughness/stiffness in a variety of epoxy/layered silicate composites with different extents of exfoliation, i.e., conventional, intercalated, and exfoliated systems. They suggested that the exfoliated
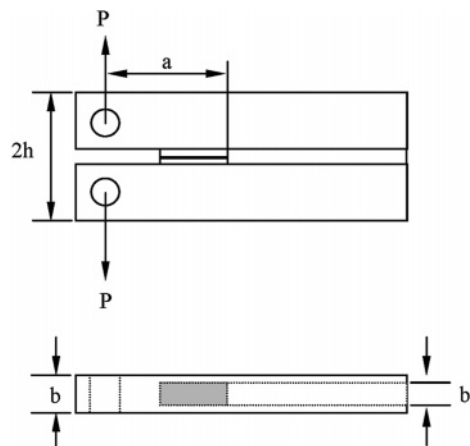
* Corresponding author.
† Institute of Materials Research and Engineering.
‡ E-mail: k-wang@imre.a-star.edu.sg.
§ E-mail: l-chen@imre.a-star.edu.sg.
⊥ Hong Kong University of Science & Technology. E-mail: mejswu@ust.hk.
|| E-mail: ml-Toh@imre.a-star.edu.sg.
E-mail: cb-he@imre.a-star.edu.sg.
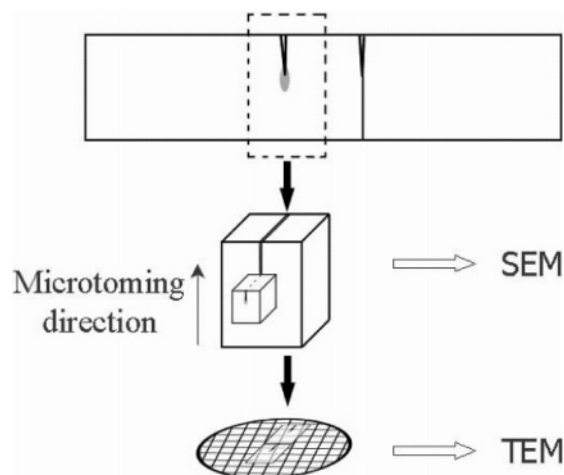○ University of Michigan. E-mail: afyee@umich.edu.

Figure 1. Diagram of the DCB specimens used in this work. Top: Side view. Bottom: Top view.

structure mainly leads to an improved modulus, while the remaining stacked structure of intercalated clay platelets is the key to improve toughness. Platelets are proposed[10] to produce nanovoids and initiate shear yielding of the epoxy interlayers at the tip of the propagating crack and also throughout the entire volume. These mechanisms, however, are only speculations as no evidence was presented. Zerda et al.[11] studied the roughness of the fracture surface and crack propagation under subcritical loadings. They suggested that the creation of additional surface area on crack propagation is the primary toughening mechanism. Kornmann et al.[15] and Kinloch et al.[16] also noticed that the fracture toughness of the epoxy/clay nanocomposite is lower than that of microcomposites. They suggested that the toughening effect is due to crack deflection and plastic deformation initiated around the particles, which lead to the formation of cavities.[16] The lower fracture tough-

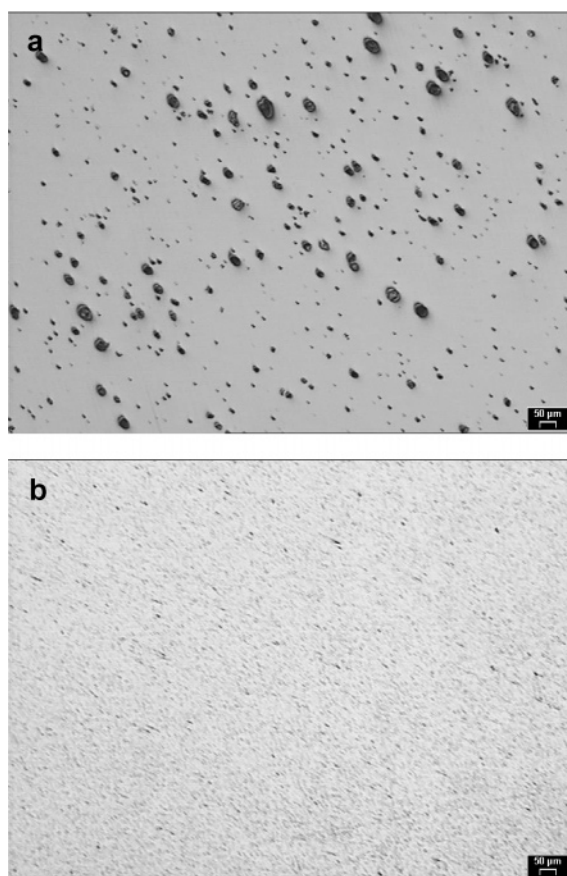**Figure 2.** Scheme of TEM sampling processes at the crack tip.

Figure 3. Optical micrographs of polished surface of the epoxy/clay nanocomposites: (a) epoxy/93A2.5; (b) epoxy/S-clay2.5 (scale bar: 50 μm).

Figure 4. TEM micrographs of the epoxy/93A2.5.

ness of nanocomposites was attributed to the larger size and lower aspect ratio of the aggregates. The platelets in these nanocomposites[15,16] were shown to retain their stacked-layer structure, although the d spacing may have been expanded considerably. Thus, the layered silicates are dispersed in the epoxy matrix as swollen microaggregates, rather than randomly distributed layers. These microaggregates are large and have low aspect ratios, which leads to a relatively smaller toughening effect.[11,12]

Knowledge of the fracture, microdeformation and mechanics of nanocomposites is rather vague. This could result from varied nanocomposite preparation tech-
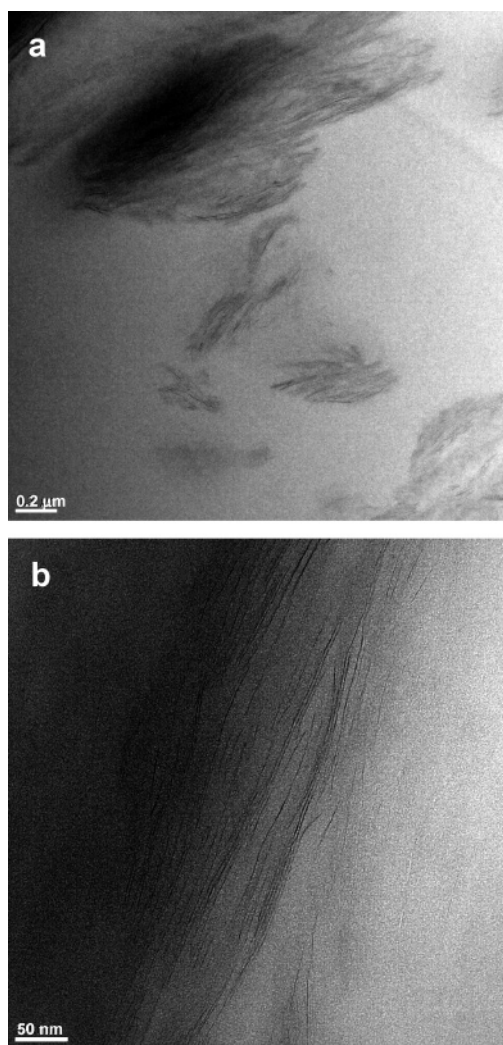
niques and the inability to obtain consistent microstructures. This difficulty is more apparent in polymer/clay systems, where clay exfoliation and homogeneous dispersion still remain as the key challenges. In most cases, clay particles exhibit intercalated rather than exfoliated structures, except in a few cases where the nanocomposites were prepared via in situ polymerization.[6] Often large aggregates of clay are observed in the material, which serve as the stress concentrators that lead to premature and brittle failure.

Recently, a new "slurry-compounding" process for the preparation of epoxy/clay nanocomposites has been developed in our group. Using this new approach, a series of epoxy/clay nanocomposites with highly exfoliated and uniformly dispersed morphology were fabricated, which enabled us to conduct a systematic investigation on the fracture toughness and microdeformation mechanisms of nanocomposites. In the present paper, the microstructure, mechanical properties, and fracture behavior of these epoxy/clay nanocomposites are presented, and their microdeformation and toughening mechanisms are discussed.

Experimental Section

Materials. Two types of clay were used in this study. one is sodium montmorillonite (PGW) from Nanocor Inc., with a cation exchange capacity (CEC) of 145 mequiv/100 g, an aspect ratio of 200−400, a d_{001} spacing of 12.5 Å and a specific density
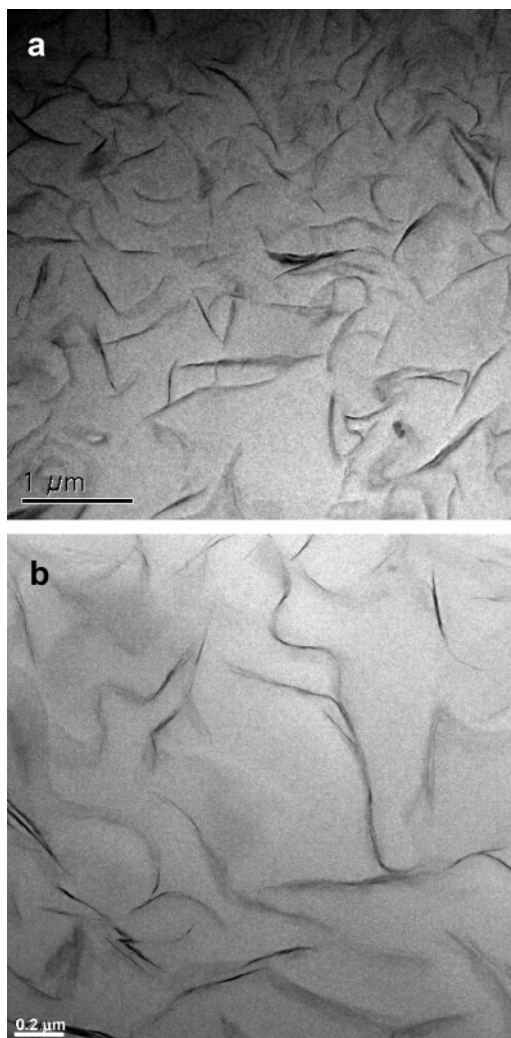
Figure 5. TEM micrographs of the epoxy/S-clay2.5.

of 2.6 g/cm³. Another one is an organoclay, Cloisite 93A from Southern Clay Corp. Cloisite 93A is a methyl dihydrogenated tallow ammonium montmorillonite. The hydrogenated tallow is derived from natural tallow, which contains a mixture of alkanes (C_{18}/C_{16}/C_{14} of 0.65:0.30:0.05). The modifier concentration is 0.9 mequiv/g of clay. The weight loss of Cloisite 93A on ignition is 40 wt %. The density is 1.88 g/cm³ and the d_{001} spacing is 23.6 Å. The epoxy is Dow Plastics Der332, a bisphenol A diglycidyl ether (DGEBA). The epoxide equivalent weight is 171−175 g/equiv. The curing agent is Ethacure 100-LC of Albemarle Corp., which is a mixture of two diethyltoluenediamine (DETDA) isomers (75−81% 2,4-isomer and 18−20% 2,6-isomer). The coupling agent, 3-glycidoxypropyltrimethoxysilane (GPTS), was purchased from Aldrich and was used as received.

Preparation of Nanocomposites. Pristine clay (4 g) was dispersed into 120 mL of deionized water to form a suspension, which was stirred at room temperature for 24 h and sonicated for 30 min. The suspension was poured in 800 mL of ethanol and stirred vigorously for 5 min. A white precipitate formed, which was filtered and washed three times with ethanol. The wet product was added to 80 mL of ethanol to form a clay/ethanol slurry. GPTS (0.2 g) was added into the slurry. The slurry was stirred for 10 h and sonicated for 30 min at room temperature. Afterward, the slurry was mixed with specific quantities of epoxy resin at 50 °C and stirred for 2 h. Ethanol was evaporated by drying in a vacuum oven at 50 °C, 3 mmHg for 48 h. Then stoichiometric quantity (Der332:100-LC = 3.8:1 by weight) of the curing agent was added, and the mixture was stirred and degassed under vacuum at 75 °C for 60 min. Finally the mixture was cured at 100 °C for 2 h and post-cured

at 180 °C for 5 h. The method is referred as a "slurry-compounding" process because the dispersion and exfoliation of clay were accomplished in the presence of solvents. Hereafter, the nanocomposites prepared using the "slurry-compounding" process with 1.0, 2.5, 3.5, and 5.0 wt % of pristine clay are designated as epoxy/S-clay1.0, epoxy/S-clay2.5, epoxy/S-clay3.5, and epoxy/S-clay5.0, respectively.

For comparison, epoxy/organoclay nanocomposites were prepared by mixing the same epoxy resin and Cloisite 93A at 75 °C for 120 min with a mechanical stirrer at a rotation speed of 800 rpm. Then, a stoichiometric quantity of the curing agent was added. The mixture was stirred, degassed and cured as described above. Hereafter, the epoxy/Cloisite 93A nanocomposites with 1.0, 2.5, and 5.0 wt % of Cloisite 93A are designated as epoxy/93A1.0, epoxy/93A2.5, and epoxy/93A5.0, respectively.

Microstructure. The dispersion of clay in nanocomposites was studied with an Olympus optical microscope. The surface of the samples was polished using SiC grinding paper (up to grit 800) and then diamond paste (up to 0.3 μm). The state of clay exfoliation in nanocomposites was observed with a transmission electron microscope (TEM). Samples were cut using a Leica Ultracut UCT ultramicrotome. Microtomed thin sections were collected on 200 mesh copper grids and examined by a Philips CM300 TEM at 300 kV in bright field mode.

Mechanical Properties. The Young's modulus and tensile strength of the nanocomposites were determined on an Instron 8800 microforce tester at a crosshead speed of 1 mm/min according to ASTM D-638. Dog-bone bars (Type V, gauge size 7.62 × 3.18 ×3.0 mm) were machined with a Ceast contour cutter.

The storage modulus and glass transition temperature (T_g) of the nanocomposites were measured with a TA 2980 dynamic mechanical analyzer by using single cantilever mode. The geometry of the specimens is 35 mm (length) × 10 mm (width) × 3 mm (thickness). Scans were conducted in a temperature range of 30 to 250 °C at a heating rate of 3 °C/min and a frequency of 1 Hz.

Fracture Toughness. (a) Single-Edge-Notch 3-Point-Bend (SEN-3PB) Tests. The Mode-I critical stress intensity factor (K_{IC}) was measured using SEN-3PB geometry (span = 50.8 mm) and single-edge-notched (SEN) specimens of 60 × 12.7 × 3.0 mm³, which meets the plane strain condition requirements.[17] A sharp notch was introduced by pressing a fresh razor blade at the bottom of a saw-slot in the middle of the rectangular bar with the Instron 8800 at a crosshead speed of 0.5 mm/min. The tests were conducted on the same Instron 8800 at a crosshead speed of 1 mm/min. K_{IC} values were calculated using[18]

$$K_{IC} = Y\frac{3PS\sqrt{a}}{2BW^2} \qquad (1)$$

$$Y = 1.93 - 3.07(a/W) + 14.53(a/W)^2 - 25.11(a/SW)^3 + 25.80(a/W)^4 \quad (2)$$

where Y is a shape factor, P the load at failure, S the length of the span, a the crack length, and W the width of the specimen.

Critical strain energy release rates (G_{IC}) were calculated from the stress intensity values using the following relationship

$$G_{IC} = \frac{K_{IC}^2}{E}(1 - \nu^2) \qquad (3)$$

where E is Young's modulus. ν is Poisson's ratio, and a typical value of 0.35[19] was used here.

(b) Double Cantilever Beam (DCB) Tests. DCB tests were performed using the Instron 8800 at a crosshead speed of 0.5 mm/min, following the method described in ref 20. The geometry of the DCB specimens is shown in Figure 1. The specimen is 6.0 mm wide, 28.8 mm thick and 72 mm long. Side
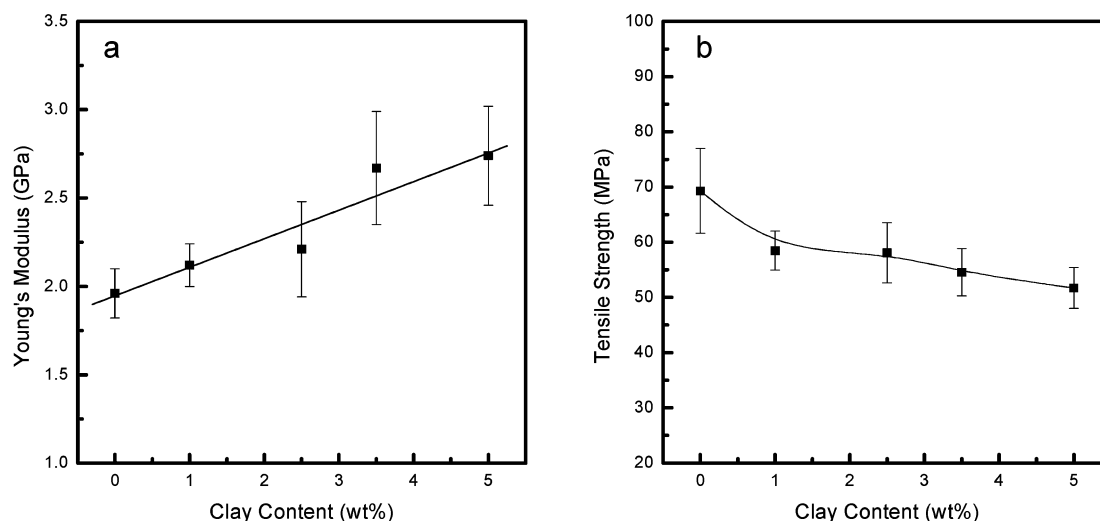
Figure 6. Mechanical properties of the epoxy/S-clays vs clay concentration. Left: Young's modulus. Right: tensile strength.
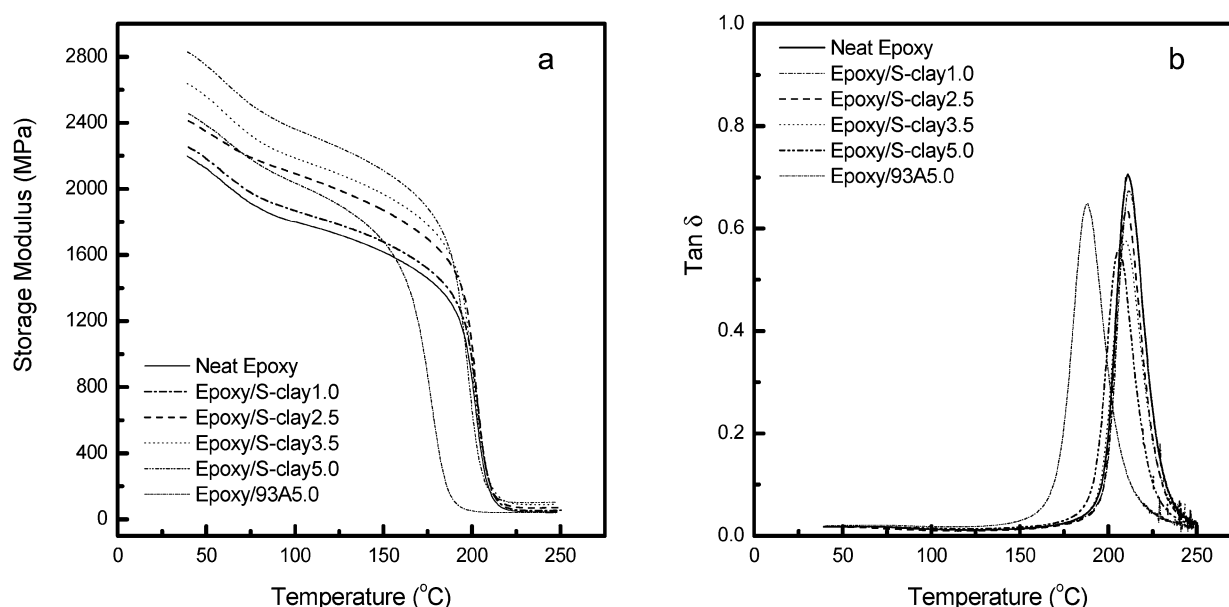

Figure 7. Storage modulus, E' (a), and tan δ (b) vs temperature for the epoxy/S-clays and epoxy/93A5.0.

grooves of depth 1.6 mm in the midplane of the specimen were used to guide the crack propagation. A precrack about 17 mm long with a sharp crack tip was made by pressing a fresh razor blade into the bottom of a machined slot. A video-recording system was used to monitor the crack propagation process.

The Mode-I critical strain energy release rate (G_{IC}) was determined from[20]

$$G_{IC} = \frac{12P^2(a + 0.668h)^2}{b_n E b h^3} \tag{4}$$

where P is the applied load, a is the crack length, b is the specimen width, b_n is the crack width, E is Young's modulus and h is the specimen half-thickness.

Fractography. Scanning electron microscope (SEM) was employed to examine the fracture surface of the tested SEN-3PB specimens. The samples were coated with a thin layer of gold and observed using a JEOL 6700F SEM. The accelerating voltage was 5 kV.

Microstructure of Crack Tips and the Damage Zone. To study the microdeformation mechanism of the epoxy/clay nanocomposites, a widely used single-edge-double-notched 4-point-bend (SEDN-4PB)/petrographic thin-sectioning technique[21-25] was performed. As illustrated in Figure 2, two identical precracks were made on one side of a bending bar,

after the sample was loaded using a four-point bend fixture. One precrack propagated through the ligament while another one was arrested in a subcritical condition. The block containing the arrested crack tip was cut and subsequently trimmed to the middle section followed by a rectangular mesa trimming using a microtome.[26] Ultrathin sections were carefully cut at 0.2 mm/s with a diamond knife using a Leica Ultracut UCT ultramicrotome. Then the sections were collected on 200 mesh carbon coated copper grids and examined by a Philips CM300 TEM at 300 kV in bright field mode. The trimmed rectangular mesa was coated with a thin layer of gold and observed using a JEOL 6700F SEM with an accelerating voltage of 5 kV. A propagated stable crack obtained using double cantilever beam (DCB) technique was also probed by TEM and SEM, and the sample was prepared using the same thin sectioning technique described.

Results and Discussion

Microstructure. The typical optical micrographs of the epoxy/S-clay and the epoxy/93A nanocomposites are shown in Figure 3. In the epoxy/93A2.5, the dispersion of organoclay is poor and the aggregate size is about 10−20 μm (Figure 3a). In the epoxy/S-clay2.5 prepared with the new approach, clay particles are uniformly
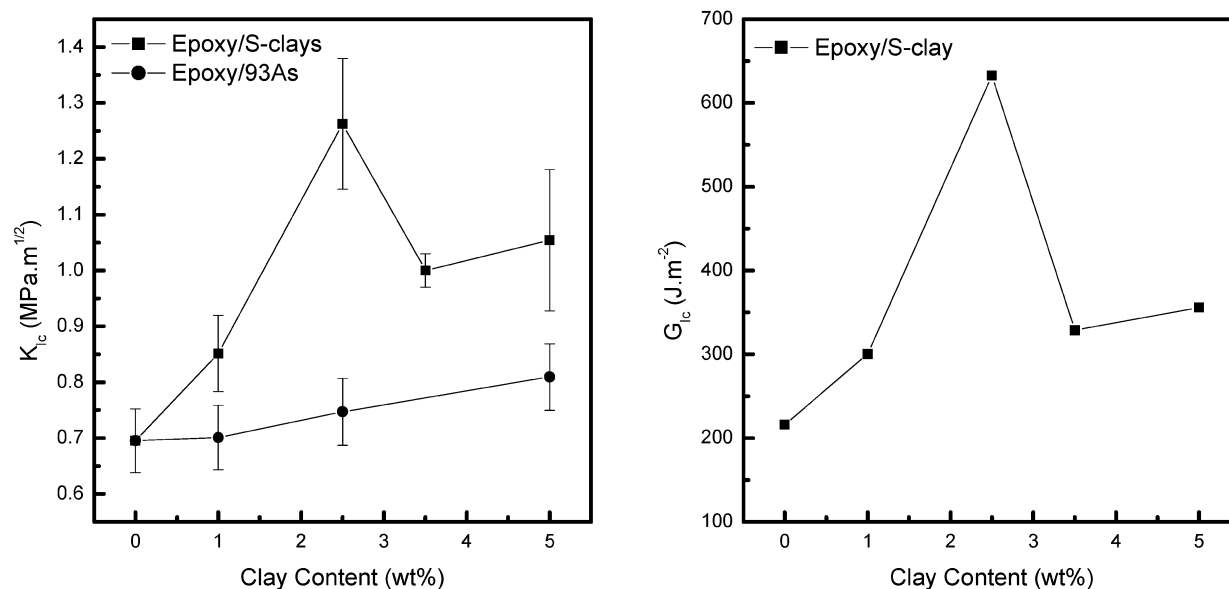
Figure 8. Fracture toughness of the epoxy/S-clays obtained with SEN-3PB as a function of clay concentration.
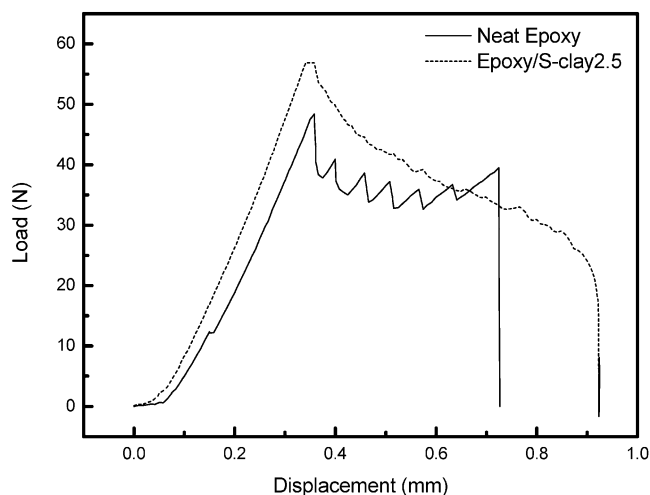

Figure 9. Typical DCB load−displacement curves of the neat epoxy and the epoxy/S-clay2.5 under continuous load.

dispersed in the matrix and the size of the aggregates is less than 3 μm (Figure 3b).

Parts a and b of Figure 4 display typical TEM micrographs of the epoxy/93A2.5. The organoclay forms aggregates although the clay stacks have been intercalated by epoxy. This morphology is typical in epoxy/organoclay nanocomposites, in which there are often more than 50 layers in each tactoid and where the ordered structure of the clay layers remained intact.[10−13] This indicates that the clay tactoids were merely swollen by the macromolecules.

The epoxy/S-clays show a completely different morphology. Parts a and b of Figure 5 display that clay is exfoliated into thin tactoids that contain only a few clay layers. These thin tactoids disperse uniformly and randomly in the matrix, indicating that the new approach is effective to promote both the exfoliation and dispersion of clay.

Tensile Testing. The incorporation of clay into epoxy resin improved its modulus considerably. As shown in Figure 6a, Young's modulus of the epoxy/S-clays increases monotonically with clay loading. A clay loading of 5 wt % improves the modulus from 1.96 to 2.74 GPa. The tensile strength of the epoxy/S-clays decreases

slightly with the increase of clay content (Figure 6b). Several reasons are possible for the decrease in tensile strength. One is the flaws existing in the nanocomposites. These flaws include the weak boundaries between particles and the bubbles trapped during the sample preparation.[15,27] The number of these flaws may increase with the volume fraction of the filler. Another possibility is the inhomogeneous network density of the samples.[10] During the preparation of the nanocomposites, the viscosity of the epoxy/clay mixture was very high due to the dramatically increased interfacial area and interfacial interaction between the highly exfoliated clay and the epoxy resin. This high viscosity would inevitably introduce heterogeneity in the resultant samples.

Dynamic Mechanical Analysis. The storage moduli (E') and tan δ values of the neat epoxy and the epoxy/S-clays are plotted against temperature in Figure 7, parts a and b, respectively. In accordance with the results of tensile tests, the E' of the epoxy/S-clays increases with the clay concentration. At temperatures higher than T_g, the improvement of E' is more dramatic.

The epoxy/93A5.0 sample shows an E' comparable with that of the epoxy/S-clay2.5 at temperatures below 100 °C (Figure 7a). This is quite reasonable because the Cloisite 93A contains about 40 wt % of organic modifier and thus the true content of clay in the sample is about 3 wt %. It is notable that the T_g of the epoxy/93A5.0 is considerably lower than that of the neat epoxy (188.0 vs 211.1 °C), and the E' of the sample decreases dramatically with the increase in temperature. On the other hand, the T_g values of the epoxy/S-clays are very close to that of the neat epoxy. With the increase of clay content, only a slight decrease of T_g can be observed.

Fracture Toughness. (a) SEN-3PB. Figure 8 displays the fracture toughness obtained by SEN-3PB tests. The K_{IC} and G_{IC} values of all epoxy/S-clays are higher than that of the neat epoxy, showing significant toughening effect. The epoxy/S-clay2.5 exhibits the highest toughness, i.e., 1.26 MPa·m$^{1/2}$ and 632 J/m^2 for K_{IC} and G_{IC}, respectively. These are much higher than the corresponding values of the neat epoxy, 0.70 MPa·m$^{1/2}$ and 216 J/m^2, respectively.
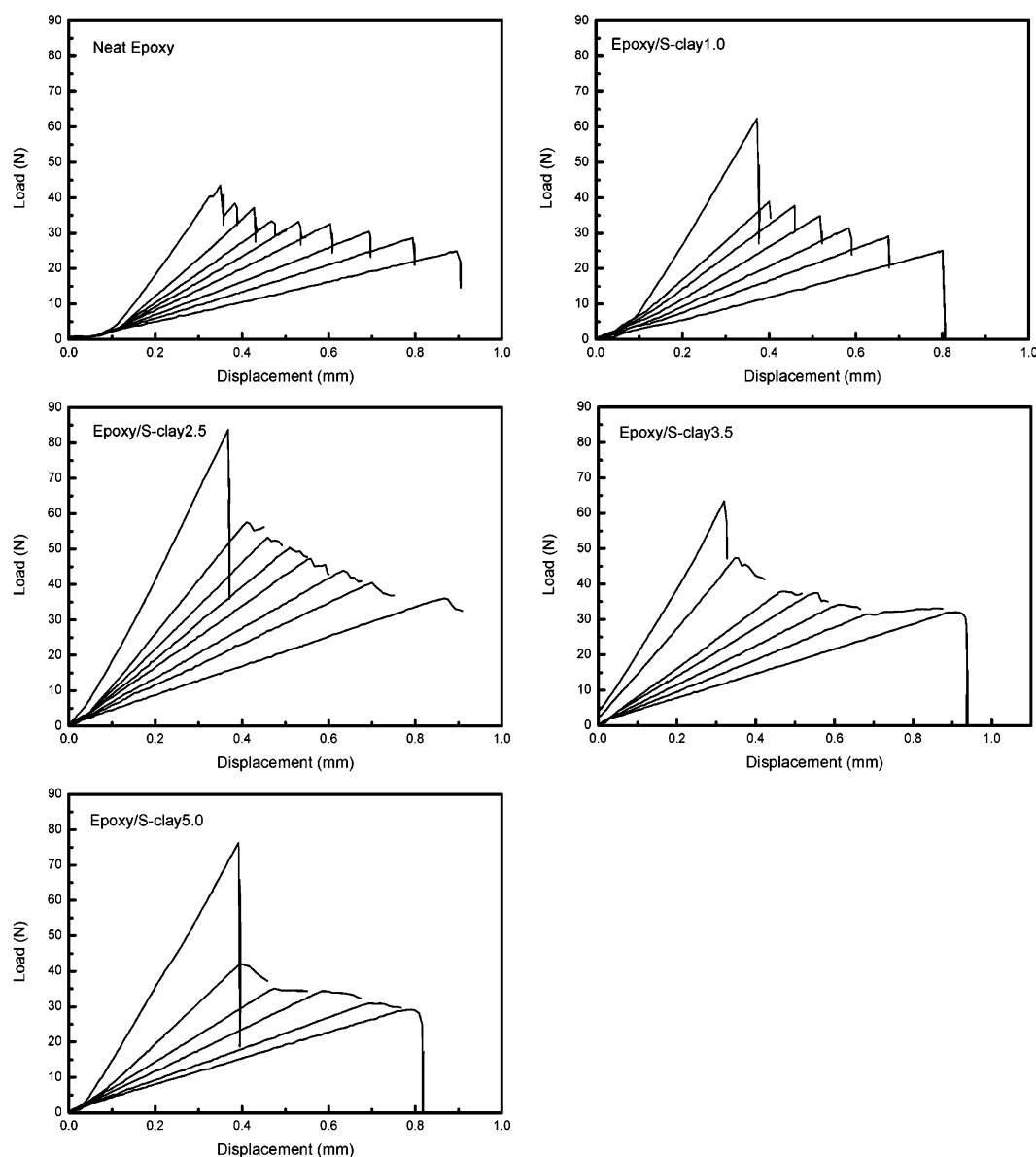
Figure 10. DCB load-displacement plots of the neat epoxy and the epoxy/S-clays after load−unload−reload cycles.
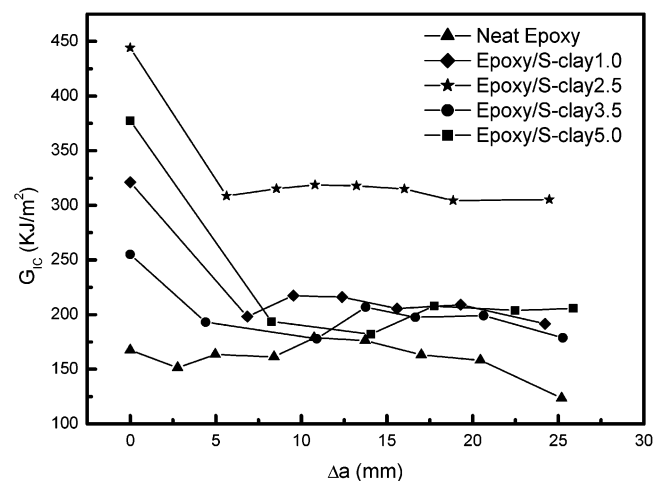

Figure 11. Plots of fracture toughness, G_{IC} against crack extension, Δa.

Figure 12. Comparison of the dependency of fracture toughness G_{IC} on clay content obtained with SEN-3PB and DCB tests.

Organoclay, Cloisite 93A, is not as effective as the clay in epoxy/S-clays in toughening epoxy. The K_{IC} values of the epoxy/93As increase monotonically with clay load
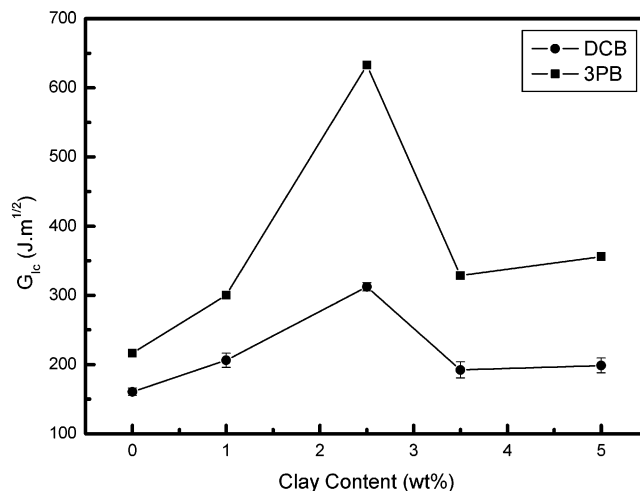
and they are always lower than that of the epoxy/S-clay nanocomposites with same clay load. This is evident
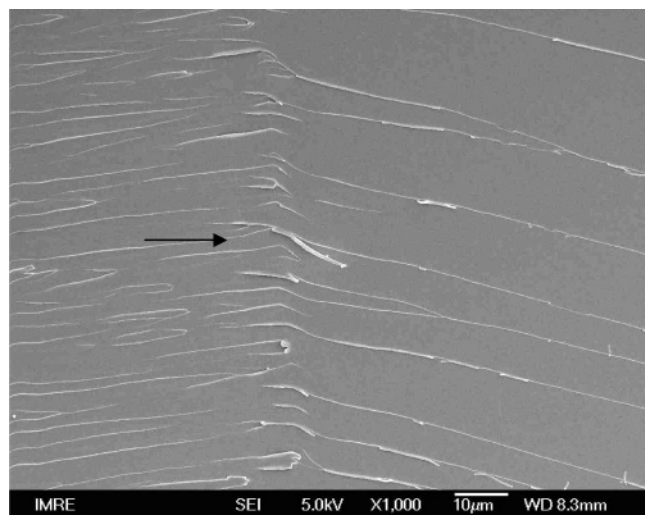
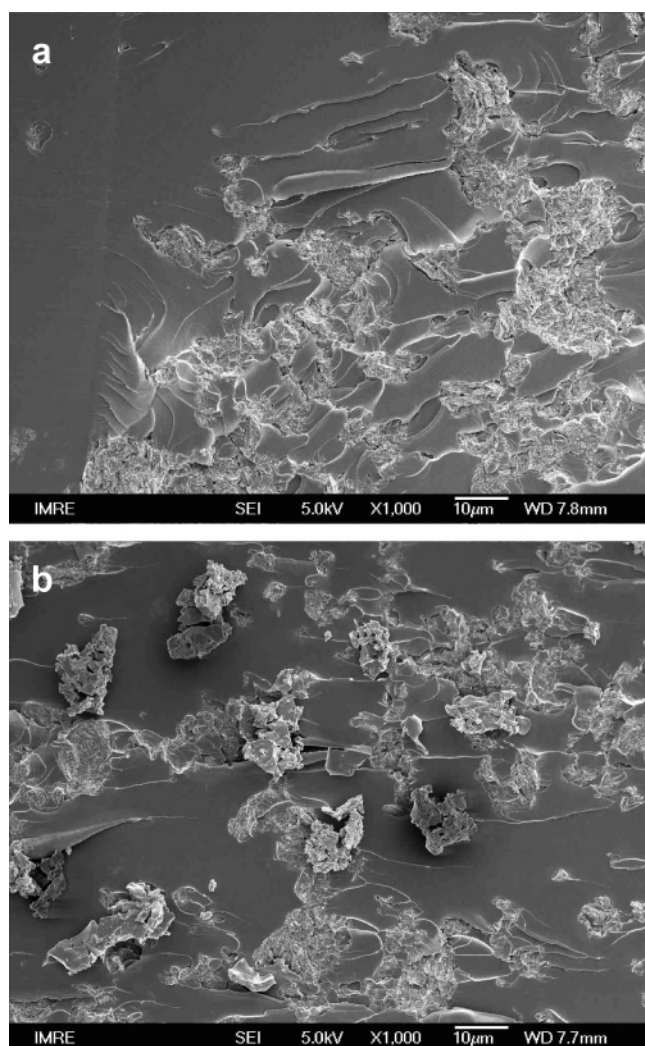**Figure 13.** SEM micrographs of the fracture surface of the neat epoxy.

Figure 14. SEM micrographs of the fracture surface of the epoxy/93A2.5: (a) crack initiation site; (b) fast-fracture region.

Figure 15. Transmitted light optical micrographs of a thin section taken near the subcritically loaded crack in the epoxy/93A2.5: (a) region analyzed without polarizers; (b) the same region as that in part a, but analyzed with crossed polarizers.

from Figure 8a, in which the K_{IC} values of both the epoxy/S-clays and the epoxy/93As are plotted against clay content.

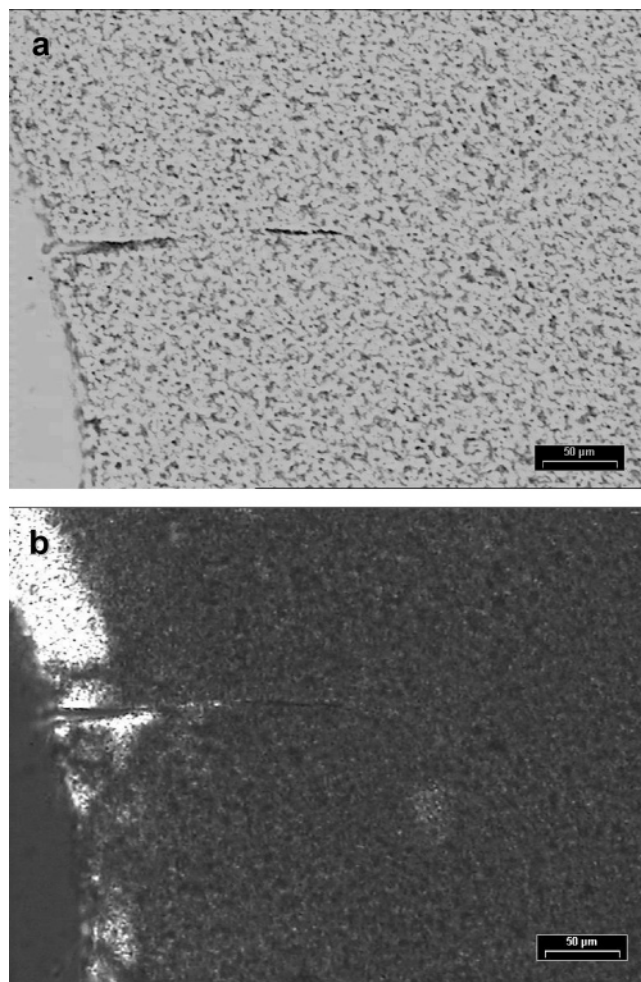**(b) Double Cantilever Beam Tests.** The fracture toughness of materials can be evaluated with different methods, e.g., SEN-3PB, compact tension (CT), DCB tests, etc. DCB specimens have the advantage that crack propagation can be controlled, which can provide more information regarding fracture mechanisms.

The DCB tests followed two loading programs: continuous loading by a constant rate of crosshead separation and load−unload−reload. Under continuous loading conditions, the crack propagation in the epoxy is unstable and exhibits a sawtooth-shaped curve (Figure 9), characteristic of the stick−slip mode of crack propagation. The epoxy/S-clay1.0 shows a similar behavior. In contrast, the epoxy/S-clays containing 2.5 wt % of clay or more exhibit stable crack propagation (Figure 9).

For samples exhibiting unstable crack growth, the crack length can be easily correlated to the load by measuring the positions of the striations on the fracture surface.[20] However, because most of the epoxy/S-clays exhibit stable crack propagation when subjected to continuous loading, it is very difficult to identify the crack length accurately using this method. To overcome this difficulty, the specimen was unloaded when some crack growth was observed. The position of crack tip was marked. Then the specimen was reloaded to induce further crack growth and unloaded again to mark the new crack tip position. This process was repeated until catastrophic fracture occurred.

The load−displacement curves of the load−unload−reload cycles are overlaid and shown in Figure 10. For the neat epoxy and the epoxy/S-clay1.0, the peak load
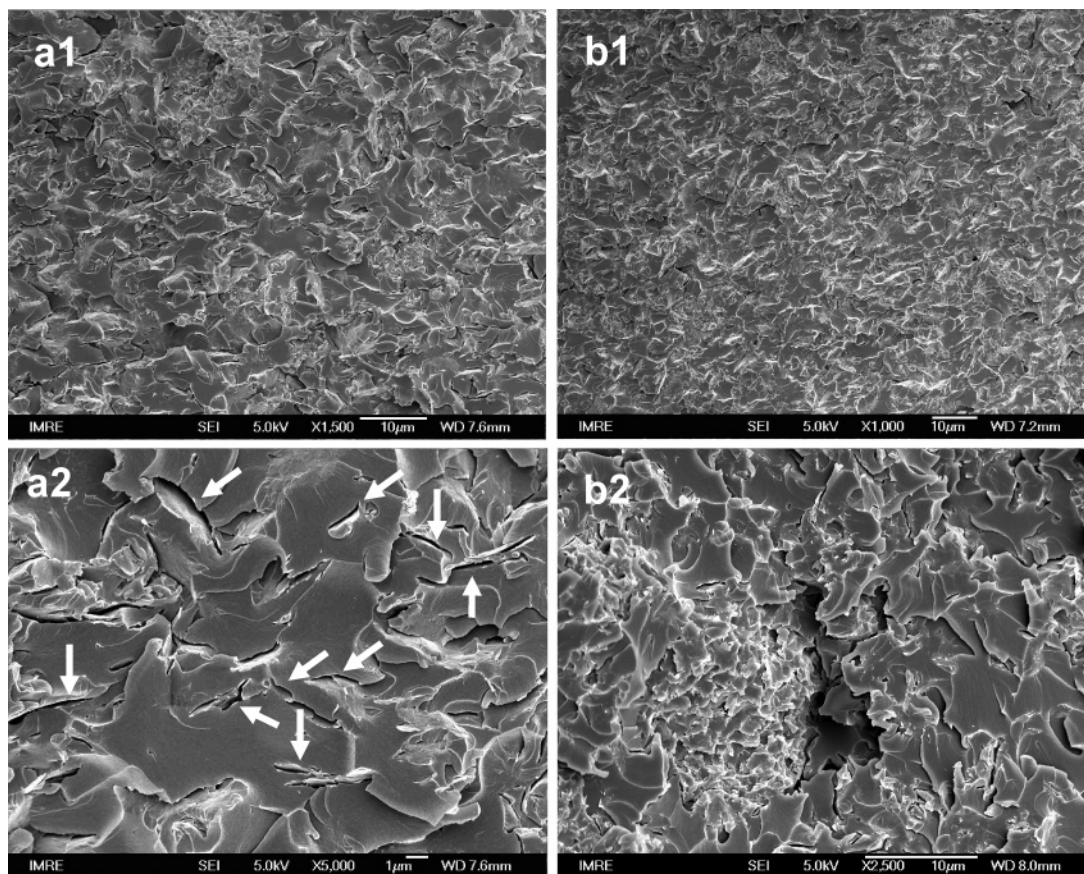
Figure 16. SEM micrographs of the fracture surface of the epoxy/S-clay2.5; (a1, a2) crack initiation site; (b1, b2) fast-fracture region.

of every cycle is followed by a sharp drop in load, indicating the pop-in of the cracks. For the samples containing more than 2.5 wt % of clay, however, only the first cycle shows such a behavior. In the rest of load−unload−reload cycles, the load decreases gradually after the peak load, showing stable crack propagation manner.

The fracture toughness G_{IC} obtained from the DCB tests is plotted against crack extension in Figure 11. The peak loads of the first cycles and the corresponding G_{IC} values calculated are much higher than those for the rest of the load cycles for each specimen. This is probably related to the preparation of precracks; viz., the precracks made with razor blade may have a fully developed (or near fully developed) damage zone caused by the razor insertion, thus the precrack was not sufficiently sharp. On the other hand, the neat epoxy is very brittle and the pop-in of the crack occurred when razor was inserted, so that the precrack is sharp enough. Therefore, for the neat epoxy, the G_{IC} value obtained in the first load cycle is consistent with that of the rest cycles.

The G_{IC} data obtained from the DCB tests are averaged and plotted against clay content in Figure 12, in which the data of first cycles are excluded. The following salient features are observed from Figures 11 and 12: (1) the epoxy/S-clays exhibit higher toughness than that of the neat epoxy, and the toughness-clay load dependency obtained by DCB is the same as that obtained by SEN-3PB testing; (2) the epoxy/S-clays with 2.5 wt % clay has the highest fracture toughness at any give crack extension; (3) there is no *R*-curve behavior in either the neat epoxy or the epoxy/S-clays (i.e., the toughness does not increase with crack length).

Fractographic Analysis. The fracture surface of the neat epoxy is very smooth except for some river line markings near the crack initiation site, as indicated by the arrow in Figure 13. The fractograph is typical for brittle polymers, revealing that the resistance to crack propagation is very low. Compared with that of the neat epoxy, the fracture surface of the epoxy/93A2.5 is rougher (Figure 14). The organoclay is poorly dispersed and forms aggregates. Aggregates are exposed on the surface because the cracks penetrated through them. Characteristic tail structures formed behind the aggregates in the process zone on the fracture surface, which are often observed in particulate filled epoxy systems.[28] The tail structures are in reality steps, which are formed when two secondary crack fronts divided by the aggregates meet with each other. With an increase of organoclay content, the aerial density of the steps increases.

Shear banding is frequently reported as one of the major toughening events in epoxy-based composites or blends.[29] Shear yielding of the matrix, if it occurs, can be observed with thin sections under polarized light, which reveal the birefringence due to plastic deformation. However, such a mechanism is not found in the current epoxy/93As. Figure 15 displays optical micrographs of thin section of a subcritical crack tip by using the method introduced by Yee and Sue.[30] No sign of shear yielding can be observed, either at the crack tip or near the process zone.

Thus, in the epoxy/93As, the improvement of the toughness can be attributed to step formation and the breakage of the clay aggregates. However, neither of these toughening mechanisms is effective enough to cause a remarkable increase of toughness.
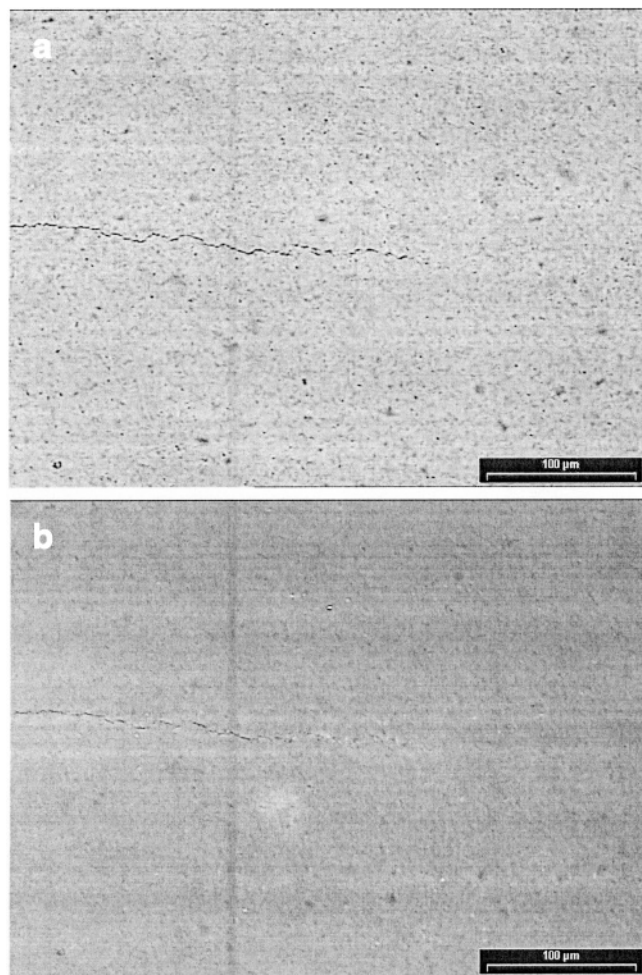
Figure 17. Transmitted light optical micrographs of a thin section taken near the subcritically loaded crack in epoxy/S-clay2.5 (a) region analyzed without polarizers; (b) the same region as that in part a, but analyzed with crossed polarizers.

The SEM fractographs of the epoxy/S-clay2.5 are shown in Figures 16. The fracture surface is very rough and filled with scalelike steps, indicating that the presence of nanoclay layers forced the crack to propagate along a very tortuous path. Under higher magnification (Figure 16a2) many microcracks are observed located between the scalelike steps (indicated by the arrows), which are perpendicular to the fracture surface.

This implies that the clay layers acted as stress concentrators and promoted the formation of a large number of microcracks when the sample was loaded. Consequently, the size of the process zone is larger than that of the neat epoxy.

Some clusters are observed in which the concentration of clay is higher than the neighboring region (Figure 16b2). Macrocracks are observed at the interfacial region, revealing that the physical properties (such as modulus and Poisson's ratio) inside and outside the clusters are different. This suggests heterogeneity results in more stress concentrations.

Figure 17 shows the optical micrographs of thin section of a subcritical crack tip of epoxy/S-clay2.5. Again, no trace of birefringence can be observed, either at the crack tip or near the process zone. However, the crack trajectory is quite tortuous, which is consistent with the SEM micrographs of fracture surface.

Electron Microscopy Study of Crack Initiation with the SEDN-4PB Specimen. According to the foregoing, the formation of a large number of microcracks and the increase in the fracture surface area due to crack deflection are the major toughening mechanisms in the current nanocomposite. However, there are still some questions need to be answered: Is microcracking the unique micromechanism? Where did the microcracks initiate, at the epoxy–clay interface or between clay layers? How did the microcracks develop into macrocracks? What happened around the crack tips? To answer these questions, the arrested crack tip of an epoxy/S-clay2.5 SEDN-4PB specimen was studied by means of TEM and SEM.

TEM micrographs from the vicinity in front of the arrested crack tip are given in Figure 18. Some incipient cracks consisting of several discontinuous cavities can be identified. These cavities are closely associated with clay platelets (indicated by arrows in Figure 18a). Long, narrow microcavities or microcracks associated with clay were also found in a region ahead of the arrested crack tip, as indicated by the arrows in Figure 18b. Most of the microcracks seem to have formed either along the matrix-clay interface or inside the clay platelets via delamination.

Artifacts introduced by TEM sample preparation may be thought to cause the microcracks formation.[31] Therefore, the diamond knife trimmed mesa containing the arrested crack tip was also examined with SEM. In the SEM micrographs presented in Figure 19, microcracks
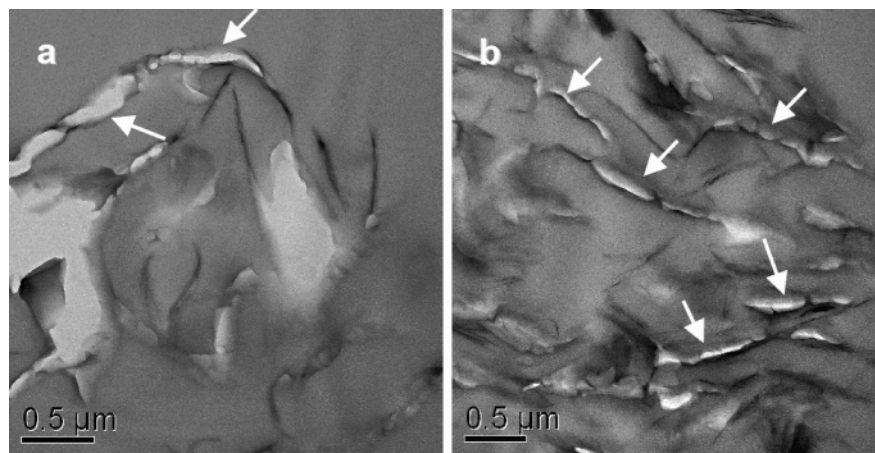

Figure 18. TEM micrographs of thin sections taken from the region in front of an arrested crack tip of epoxy/S-clay2.5.
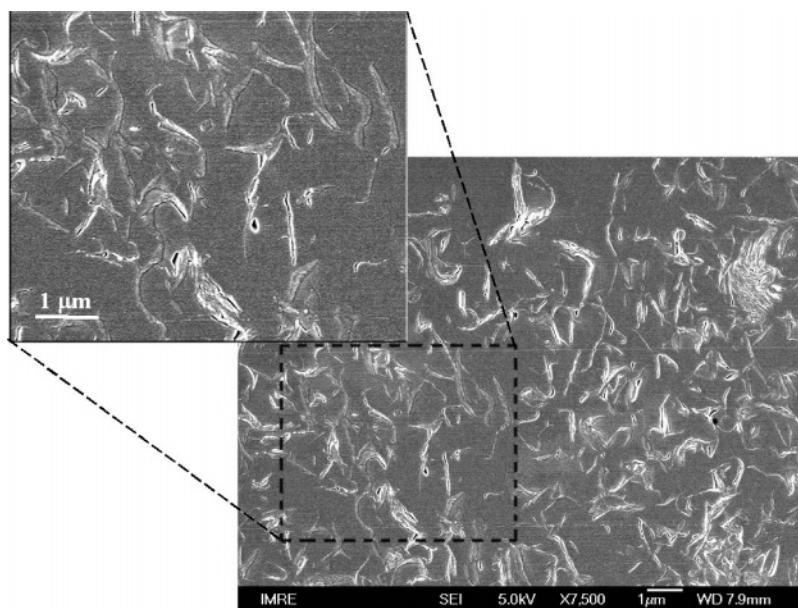
Figure 19. SEM micrographs of the damage zone trimmed with diamond knife.
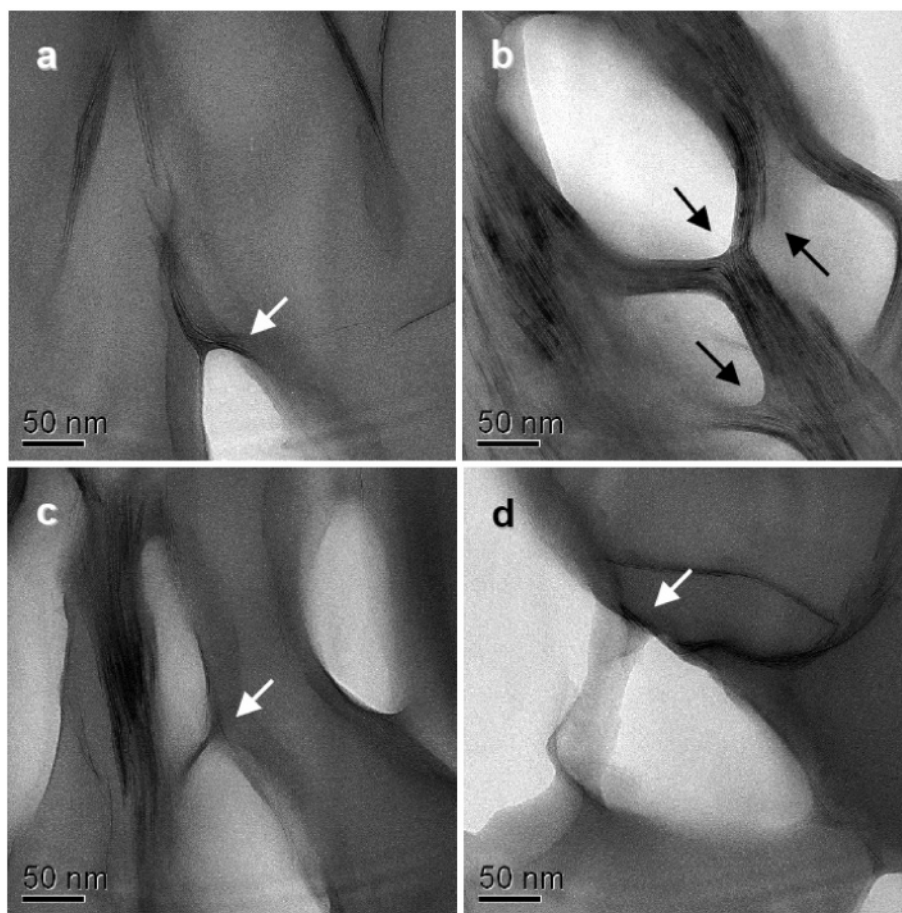

Figure 20. TEM micrographs indicating microcracks in epoxy/S-clay2.5.

with the same characteristics as found in the TEM observation are also revealed. This demonstrates that these microcracks were not artifacts of the preparation of ultrathin sections, i.e., they are the inherent features of the subcritically loaded specimen.

To study the structure of the microcracks, the samples were observed under high magnification with TEM. As shown in Figure 20, parts a and b, the microcracks were

formed between clay layers. This phenomenon characterizes most of the microcracks, revealing that these microcracks are initiated within the intergallery of clay layers rather than at the epoxy–clay interface. Similar phenomena were reported in some other clay filled polymers.[31–33] From in situ tensile tests under an electron microscope, Kim and co-workers[32] observed that the deformation starts inside the stacked silicate layers.
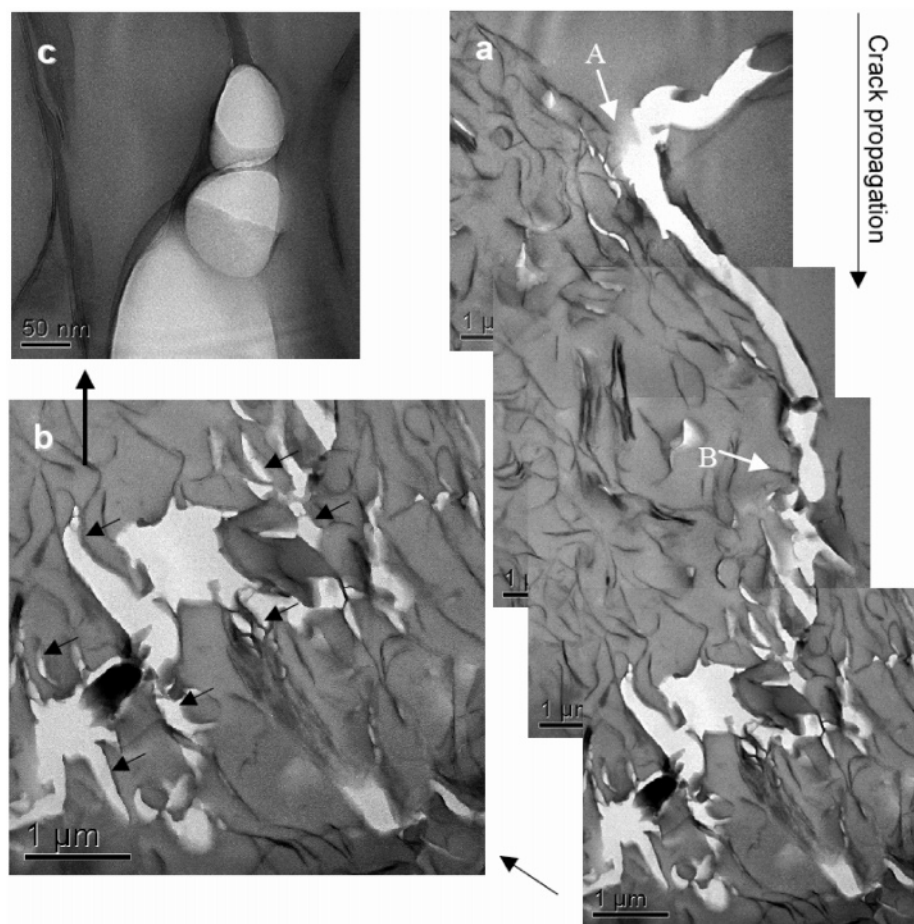
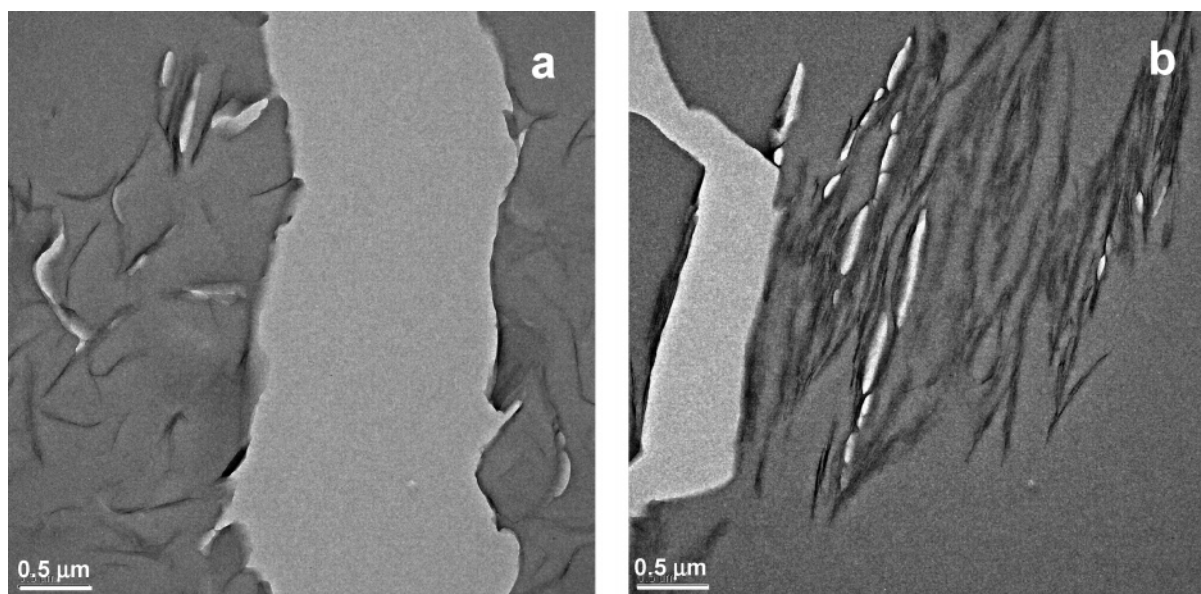**Figure 21.** TEM micrographs of a propagated crack in epoxy/S-clay2.5.

Figure 22. TEM micrographs of a propagated crack in epoxy/S-clay5.0.

Then microvoids form between the silicate layers. The weakly bonded silicate layers were believed to be the cause of the nucleation of microcracks taking place easily inside the stacked layers, rather than at the polar region.

The crack initiation process in the epoxy/S-clay nanocomposites can now be described. When the sample is subjected to a load, stress concentrates around the clay tactoids due to the difference of Young's modulus and Poisson's ratio of clay and epoxy. Because the clay interlayer strength is weaker than the epoxy−clay interfacial bonding strength and the cohesive strength of epoxy, interlaminar debonding takes place. Subsequently, microcracks form. This mechanism is further confirmed by Figure 20, parts c and d, in which some clay strips bridging the crack tip due to interlaminar debonding can be observed. With further loading, the neighboring microcracks will extend in length, penetrate
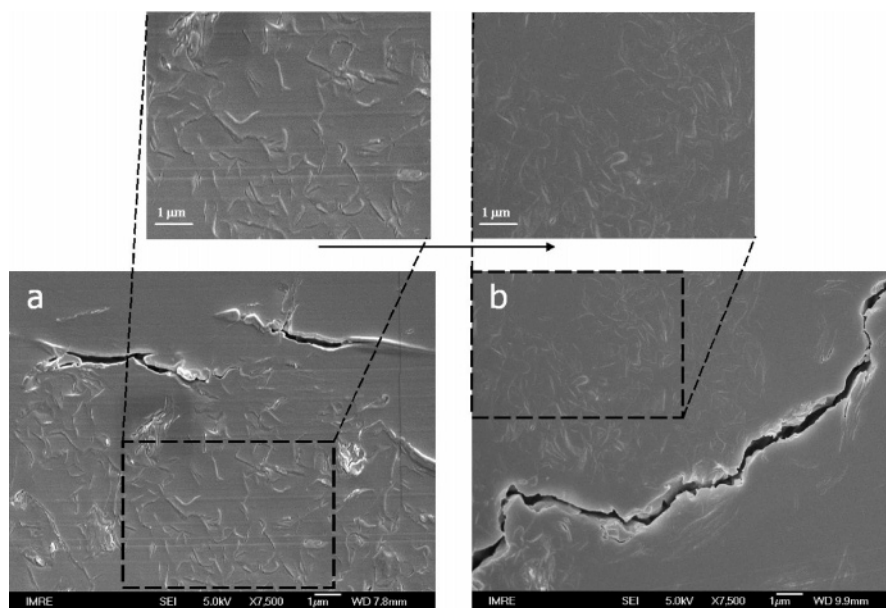
Figure 23. SEM micrographs of the diamond knife trimmed region around the arrested crack in (a) epoxy/S-clay2.5 and (b) epoxy/S-clay 5.0. The arrow indicates the crack propagation direction.
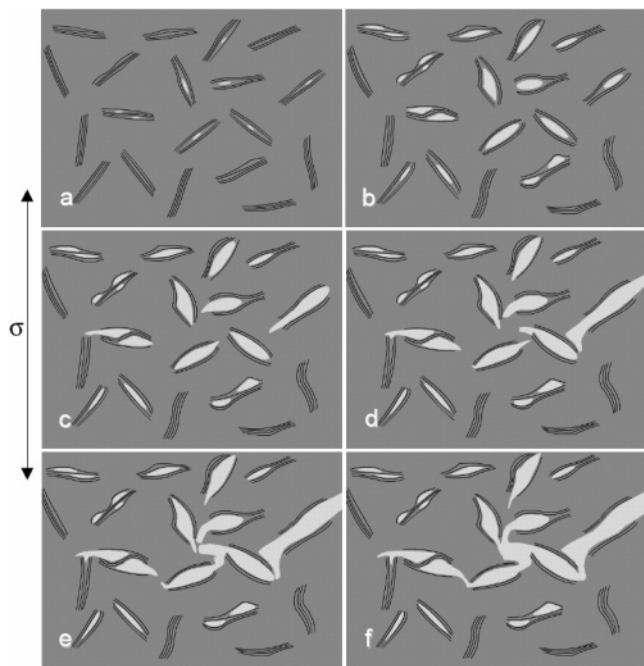

Figure 24. Illustration of the crack initiation and propagation processes in the epoxy/S-clay nanocomposites.

the matrix ligaments between them and finally develop into a macroscopic crack.

Electron Microscopy Study of Crack Propagation with DCB Specimen. The uniformly dispersed and highly exfoliated clay in epoxy matrix may resist crack propagation. There are two major ways for the crack to propagate further when its tip meets the clay layers or clusters: (1) it may penetrate inside the cluster straight away and split the cluster if the clay layers ahead the crack tip orient almost parallel to the crack propagation direction, or (2) it may bend along the region adjoining the cluster−matrix interface if the clay layers orient perpendicularly to the crack propagation direction. Whether the cracks are able to penetrate into the clay layer cluster depends on the difference between

the crack propagation direction and the clay layers' orientation.

A stable propagated crack was obtained with a DCB specimen of the epoxy/S-clay2.5 and the propagation of the crack was traced by TEM. The crack tip reached site A first (Figure 21a) where the orientation of the clay layers was almost perpendicular to that of the crack propagation direction. Evidently, the clay layers hindered the crack propagation. Although some microcracks nucleated in front of the main crack (below site A), the rigid clay layers did not break and give way to crack propagation. As a result, the crack deflected and extended outside the cluster. The crack propagation proceeded between the clay layers, and small portions of stacked clay layers appeared in the immediate vicinity of the large crack and directly connected to the new surfaces of the main crack. Such phenomena also indicate weak interlayer bonding. When the crack met a weak point within the cluster, it penetrated inside at site B where the orientation of clay layers was almost parallel to the crack propagation direction. Crack propagation in the cluster progressed by splitting clay layers, breaking matrix ligaments and merging microcracks. This resulted in many subcracks perpendicular to the main crack, as indicated in Figure 21b by arrows. These subcracks are consistent with the foregoing microcavities observed on the fracture surface. It is notable that these subcracks stopped after a very short crack extension $(1-2 \ \mu m)$ and the tip was blunted, as shown in Figure 21c. Again, it is worthwhile to mention that, there are no traces of large plastic deformation of the epoxy matrix observed near the crack.

Deformed DCB sample of epoxy/S-clay5.0 was also examined using TEM (Figure 22). Consistent with the observations in epoxy/S-clay2.5, microcracks nucleated by clay interlayer delaminating are also observed. However, the amount of the microcracking appears to be less (Figure 22a) and some large aggregates with many stacks of clay layers can be easily found (Figure 22b). The SEM micrographs of the diamond knife trimmed mesa containing arrested crack is shown in Figure 23. Microcracks can be found in a large area near

the propagated crack in the epoxy/S-clay2.5 (Figure 23a). For epoxy/S-clay5.0, however, no obvious traces of microcracks can be identified in the region about 1 μm away from the propagated crack (Figure 23b).

Therefore, the causes for the lower fracture toughness of 5 wt % clay loaded epoxy could be as follows: (1) the larger clay aggregates concentrate much high local stress that causes premature fracture; (2) according to the TEM and SEM observations of DCB specimens, the amount of microcracks is dramatically reduced at 5 wt % clay loading. Thus, the energy dissipated for microcracking would be less resulting in a lower fracture toughness.

Microdeformation and Toughening Mechanisms. The microdeformation mechanisms in highly exfoliated epoxy/clay nanocomposites, which are schematically shown in Figure 24, can be described as follows: (1) When subjected to load, some microcracks initiate inside the weakly bonded clay interlayers (Figure 24a). (2) Upon further loading, these microcracks develop and extend into the matrix (Figures 24b and 24c). (3) The cracks tend to penetrate matrix ligaments and coalesce (Figures 24d and 24e). (4) Due to the random orientation and good dispersion of the clay layers, the microcracks were not coplanar. The macroscopic crack formed from these microcracks developed from a crack propagation trajectory that was quite tortuous and had a lot of steps, hackles, as well as clefts perpendicular to the main crack (Figure 24f). On the other hand, after the macroscopic crack forms, the preformed microcracks in the sub-fracture surface may retain their state and will not develop as the neighboring main crack. This helps to release the strain energy and alleviate the triaxial tension. (5) The high load keeps the macroscopic crack propagating in a tortuous way. Finally, catastrophic fracture takes place when reaching a critical state.

In the present study, neither plastic deformation nor crack pinning effect was observed. Therefore, the formation of massive microcracks and the increase of the fracture surface area due to crack deflection are the major toughening mechanisms in the current nanocomposite.

Conclusions

A "slurry-compounding" process was developed for the preparation of epoxy/clay nanocomposites. With the new approach, clay was exfoliated into thin tactoids containing only a few layers, which disperse uniformly and orient randomly in the epoxy matrix; Both Young's modulus and the fracture toughness are improved with the incorporation of clay and the sample containing 2.5 wt % of clay shows the highest fracture toughness. However, neither diffuse shear yielding nor microshear banding was observed. The initiation and development of microcracks are the dominant microdeformation and fracture mechanisms in these nanocomposites. Most of the microcracks initiate between clay layers, which develop within the tactoids and extend into the matrix as the strain increases. The microcracks tend to penetrate through the matrix ligaments and merge together with the progress of deformation. The path of crack propagation is quite tortuous, and a lot of clefts perpendicular to the main crack are formed. Finally, some

microcracks coalesce into one major crack, and catastrophic fracture occurs. The formation of a large number of microcracks and the increase of fracture surface area due to crack deflection are the major toughening mechanisms in the epoxy/clay nanocomposite.

References and Notes

(1) Usuki, A.; Kojima, Y.; Kawasumi, M.; Okada, A.; Fukushima, Y.; Kurauchi, T.; Kamigaito, O. *J. Mater. Res.* **1993**, *8*, 1179.
(2) Messersmith, P. B.; Giannelis, E. P. *Chem. Mater.* **1994**, *5*, 1719.
(3) Lan, T.; Pinnavaia, T. J. *Chem. Mater.* **1994**, *6*, 2216.
(4) Wang, M. S.; Pinnavaia, T. J. *Chem. Mater.* **1994**, *6*, 468.
(5) Lan, T.; Kaviratna, P. D.; Pinnavaia, T. J. *Chem. Mater.*. **1995**, *7*, 2144.
(6) Giannelis, E. P. *Adv. Mater.* **1996**, *8*, 29.
(7) Konmann, X.; Lindberg, H.; Berglund, L. A. *Polymer* **2001**, *42*, 1303−1310.
(8) Kong, D.; Park, C. E. *Chem. Mater.* **2003**, *15*, 419.
(9) Park, J. H.; Jana, S. C. *Macromolecules* **2003**, *36*, 2758.
(10) Zilg, C.; Mulhaupt, R.; Finter, J. J. *Macromol. Chem. Phys.* **1999**, *200*, 661.
(11) Zerda, A. S.; Lesser, A. J. *J. Polym. Sci., Part B: Polym. Phys.* **2001**, *39*, 1137.
(12) Becker, O.; Varley, R. J.; Simon, G. P. *Polymer* **2002**, *43*, 4365.
(13) Becker, O.; Cheng, Y. B.; Varley, R. J.; Simon, G. P. *Macromolecules* **2003**, *36*, 1616.
(14) Ratna, D.; Manoj, N. R.; Varley, R.; Singh Raman, R. K.; Simon, G. P. *Polym. Int.* **2003**, *52*, 1403.
(15) Kornmann, X.; Thomann, R.; Mulhaupt, R.; Finter, J.; Berglund, L. *J. Appl. Polym. Sci.* **2002**, *86*, 2643.
(16) Kinloch, A. J.; Taylor, A. C. *J. Mater. Sci. Lett.* **2003**, *22*, 1439.
(17) Kinloch, A. J.; Young, R. J. In *Fracture behavior of polymers*; Elsevier: Amsterdam, 1985.
(18) Hertzberg, R. W. In *Deformation and fracture mechanics of engineering materials*; Wiley-Interscience: New York, 1989.
(19) Gledhill, R. A.; Kinloch, A. J.; Yamini, S.; Young, R. J. *Polymer* **1978**, *19*, 574.
(20) Du, J.; Thouless, M. D.; Yee, A. F. *Int. J. Fract.* **1998**, *92*, 271.
(21) Sue, H. J.; Yee, A. F. *J. Mater. Sci.* **1989**, *24*, 1447.
(22) Sue, H. J.; Yee, A. F. *J. Mater. Sci.* **1991**, *26*, 3449.
(23) Wong, S. C.; Mai, Y. W. *Polymer* **1999**, *40*, 1553.
(24) Wu, J.; Guo, B.; Chan, C. M.; Li, J.; Tang, H.-S. *Polymer* **2001**, *42*, 8857.
(25) Chen, L.; Wong, S. C.; Liu, T.; Lu, X.; He, C. *J. Polym. Sci., Part B: Polym. Phys.* **2004**, *42*, 2759.
(26) Reid, N In *Ultramicrotomy*; North-Holland: Amsterdam, 1975; pp 285−286.
(27) Lee, J.; Yee, A. F. *J. Appl. Polym. Sci.* **2001**, *79*, 1371.
(28) Lee, J.; Yee, A. F. *Polymer* **2000**, *41*, 8363.
(29) Lee, J.; Yee, A. F. *Polymer* **2000**, *41*, 8375.
(30) Sue, H. J.; Yee, A. F. *J. Mater. Sci.* **1993**, *28*, 2975.
(31) Gam, K. T.; Miyamoto, M.; Nishimura, R.; Sue, H. J. *Polym. Eng. Sci.* **2003**, *43*, 1635.
(32) Kim, G. M.; Lee, D. H.; Hoffmann, B.; Kressler, J.; Stoppelmann, G. *Polymer* **2001**, *42*, 1095.
(33) Manias, E.; Han, W. J.; Jandt, K. D.; Kramer, E. J.; Giannelis, E. P. In *Nanophase and Nanocomposite Materials II Symposium Held December 2-5, 1996, Boston, Massachusetts*; Komarneni, S., Parker, J. C., Wollenberger, H, Eds.; Materials Research Society Symposium Proceedings; Materials Research Society: Warrendale, PA, 1997, pp 495.